Title: Organoid-based *in vitro* systems to model *Cryptosporidium parvum* infection in 2D and 3D

Running Title: Organoid-based *Cryptosporidium* infection models

Bethany R. Korwin-Mihavics[1,2,3], Emmett A. Dews[1,2], Bruno Martorelli di Genova[2,3], Christopher D. Huston[1,2,3]

[1]Department of Medicine, University of Vermont, Burlington, Vermont, USA
[2]Microbiology and Molecular Genetics, University of Vermont, Burlington, Vermont, USA
[3]Cellular, Molecular, and Biomedical Sciences, University of Vermont, Burlington, Vermont, USA

Corresponding Author:

Christopher Huston
92 Carrigan Drive, Stafford 202B, Burlington, VT 05401
(802) 656-9115
Christopher.huston@med.uvm.edu

Abstract

Typical cancer cell-based culture systems cannot support the full life cycle of *Cryptosporidium parvum*, despite its monoxenous life cycle which is completed in the small intestine of a single host. There is a block to fertilization and zygote formation *in vitro*. In this paper, we adapted a 2D organoid derived monolayer system and a 3D inverted enteroid system for use in *C. parvum* culture. 3D inverted enteroids were successfully infected by *C. parvum* without the need for microinjection and supported subculture of *C. parvum*. Using the 2D organoid derived monolayer (ODM) system, the infection can be maintained for at least 3 weeks with new oocyst production throughout. Fertilization was confirmed based on successful mating of two strains of *C. parvum.* We demonstrated that the apparent block to fertilization in typical cell culture is overcome using ODMs.

Introduction

Cryptosporidium is a protozoan intestinal parasite transmitted by the fecal-oral route that accounts for approximately 10% of the global diarrheal disease burden [1] and is among the top 5 infectious causes of moderate to severe diarrhea in children under 2 years [2,3]. In immunocompetent adults, cryptosporidiosis is self-limited and usually resolves within 2-3 weeks, but it can develop into severe disease that can be life-threatening in immunocompromised individuals, young children (especially if malnourished), and the elderly. Unfortunately, the only available drug treatment, nitazoxanide, is poorly effective in the most vulnerable populations and there is no vaccine. Chronic or repeated infection with *Cryptosporidium* can cause intestinal damage resulting in loss of absorptive surface area and contribute to future malabsorption and malnutrition, resulting in a vicious cycle of malnutrition and infection that can result in long-term growth stunting and cognitive deficits in young children [4].

Cryptosporidium exhibits monoxenous development, whereby the entire lifecycle is completed within a single host, in contrast to many other well-known protozoan parasites such as *Plasmodium* and *Toxoplasma*. Upon ingestion, oocysts pass through the acidic stomach environment and into the small intestine where bile acids and digestive enzymes promote excystation to release motile sporozoites. Sporozoites invade the host cell, establish an epicellular niche in which the parasite is intracellular but extracytoplasmic, and develop into trophozoites that then mature into meronts containing 8 merozoites. Motile merozoites then escape and reinvade new host cells. Three rounds of merogony occur resulting in massive expansion of the parasite population [5,6]. After, merozoites differentiate into sexual stages, the microgamont (male stage) and the macrogamont (female stage) [6]. Microgamonts release microgametes which find, attach, and fuse with the macrogamont, forming a zygote which sporulates to form a new oocyst. These new, hardy, bleach-resistant oocysts are excreted and released into the environment where they wait to be ingested by a new host.

Due to its monoxenous development, a system of continuous culture should be simple, but such a system has been elusive for *Cryptosporidium*. Many approaches have been taken, and while some demonstrated support of the full life cycle, they have not been widely adopted, suggesting excessive complexity, incompatibility with study needs, or an inability to reproduce the results.

The conventional culture method using colorectal cancer cells (HCT8s) supports initial infection from the oocyst, asexual reproduction, and sexual differentiation [7]. However, It does not support the production of new oocysts, suggesting a block to fertilization and zygote formation [6]. Alternative methods using HCT8s in a candle jar or COLO-680N esophageal cancer cells were reported to support production of new oocysts and, in the latter case, sustained oocyst production for up to 8 weeks [8,9]. Additionally, hollow nanofibers lined with HCT8s produced infectious oocysts for up to 20 weeks and maintained oocyst production for 2 years, but this has not been widely adopted and is not compatible with microscopy methods [10,11].

Organoid-based infection models offer a more promising and physiologically relevant approach due to the presence of differentiated intestinal epithelial stem cells. One study using three dimensional organoids derived from human intestinal epithelial cells showed new oocyst production [12]. Although this method was compatible with microscopy techniques, it required tedious microinjection of the enteroids for the infection. Another intestinal stem cell derived system utilized a Matrigel™ scaffold in which targeted laser ablation was used to create a channel in the Matrigel™ mimicking intestinal crypts and villi to serve as a scaffold for intestinal stem cell attachment and differentiation [13]. This was reported to support *C. parvum* oocyst production for 4 weeks [13]. A stem cell derived air-liquid interface culture system was also recently described [14]. While this method has potential, it has a few disadvantages, such as requiring the maintenance of two cell lines and the long setup time, where the initial cell differentiation takes up to 11 days [14].

The methods described here have been adapted from a number of protocols [15–18] to support the full lifecycle of *Cryptosporidium in vitro* in two and three dimensions. In contrast to the previously described methods, our method uses readily available reagents and equipment to decrease the pre-infection culture preparation time, dispenses with the feeder cell line, and circumvents the need for microinjection of enteroids to model *Cryptosporidium* infection while still being representative of the intestinal environment.

Importance

This system overcomes the disadvantages of previous organoid-based methods for *Cryptosporidium* culture. It is faster and simpler than previously described systems, circumvents the need for

microinjection, uses defined media to increase reproducibility and consistency, enables real-time observation and subculture, supports parasite fertilization and oocyst production, and provides a physiologically relevant tissue culture system to facilitate studies of *Cryptosporidium* cell biology that can be implemented in 2D or 3D. Host-pathogen interactions could be interrogated from both sides by using stem cells derived from available transgenic mice in combination with parasite genetic manipulation. With small adjustments for various species, it could facilitate study of *Cryptosporidium*-host specificity. Immune responses can be investigated by incorporating co-culture of desired immune cell types or by investigating the innate immune responses stimulated in the intestinal epithelium. Two and three dimensional organoid based methods could potentially aid in elucidating previously inaccessible aspects of *Cryptosporidium*'s biology.

Results

Inverted, differentiated enteroids exhibit characteristics of the intestinal epithelium and allow infection with *C. parvum* without the need for microinjection. Previous organoid models of *Cryptosporidium* infection required microinjection for infection of the apical surface of the enteroid cells [12]. To circumvent this limitation, we inverted the polarity of the organoid cells to orient the apical surface outward (Fig. 1A). Prior to inversion, spheroids composed of mouse intestinal stem cells (mISC) were embedded in Matrigel™ with the apical surface facing inward as demonstrated by the concentration of actin on the interior surface (Fig. 1B). After removal of the extracellular matrix, brief disruption of the tight junctions, and resuspension in differentiation media (DM), the apical surface reoriented to face the exterior of the organoid within 24 hours. Initially, actin distribution appeared disordered (Fig. 1C). Organoid inversion was confirmed by the concentration of actin at the brush border near the exterior surface of the organoid. After 2-3 days suspended in DM, inverted enteroids often began to exhibit a more lobular shape while concentration of actin near the exterior surface was maintained (Fig. 1D). Transmission electron microscopy confirmed the presence of tight junctions, microvilli, and a glycocalyx on the exterior of inverted, differentiated enteroids (Fig. 1F-1G). Additionally, gene expression measured by qRT-PCR confirmed that expression of genes associated with differentiated cell types such as enteroendocrine cells (Fig. 1I) and goblet cells (Fig. 1J) was increased in inverted, differentiated enteroids, while the intestinal stem cell marker lgr5 was significantly decreased in inverted, differentiated enteroids compared to undifferentiated spheroids (Fig. 1H). Tight junction marker, ZO-1, expression was not significantly different in enteroids compared to spheroids and greater variation in ZO-1 expression was observed in inverted enteroids (Fig. 1K). Suspended enteroids demonstrated similar turnover to the intestinal epithelium. As a result, dead or dying cells may have also been included in the RNA extracted, explaining the variation in expression of ZO-1.

Successful infection of inverted enteroids with *C. parvum* was achieved by excysting *C. parvum*, adding free sporozoites to the medium, and incubating the inverted enteroids and sporozoites with intermittent agitation for 1-2 hours at 37°C. Infection was confirmed by staining parasitophorous vacuoles (PV) with FITC-conjugated *Vicia Villosa* lectin and imaging with epifluorescent microscopy (Fig. 1E). Consistent with expansion of the parasite population, more parasite DNA was detected by qPCR 7 days post infection (dpi) after addition of live vs. heat-killed parasites (Fig. 1L). Likely, the parasite DNA detected in the heat-killed condition was DNA left over from the initial input of parasites that was not removed during media changes.

Inverted enteroids support subculture of *C. parvum*. Parasites were passaged twice in inverted enteroids and infected enteroids were observed in the second passage (Fig. 2B-2E). Multiple parasite vacuoles were observed in some (Fig. 2B, H). The burden of the initial infection and first passage quantified by qPCR showed significant expansion in the live infection during the initial infection compared to the initial infection with heat killed *C. parvum* (Fig. 2F). The first passage showed significantly lower parasite counts in the live condition (Fig. 2F). This was not due to lower host cell numbers as the expression of mouse GAPDH remained similar across conditions (Fig 2G). Despite the low infection load in the first passage, parasites collected from the supernatant produced successful infection in the second passage as demonstrated by the infected enteroids in the second passage (Fig. 2B-E, H). These experiments demonstrate the feasibility of subculturing *C. parvum* in enteroids, but they also highlight that infection and reinfection efficiency in enteroids needs improvement.

Organoid derived monolayers exhibit the characteristics of differentiated intestinal epithelium and support *C. parvum* infection. Confluent mouse intestinal stem cells were grown on Matrigel coated permeable supports with 50% SCMM for the first 24 hours, 5% SCMM for the second 24 hours, and were then allowed to differentiate in differentiation media (DM) for 2 to 3 days before *C. parvum infection* (Fig. 3A). Characteristics of functional intestinal epithelial tissue, e.g., microvilli (Fig. 3J and 3K) and tight junctions (Fig. 3B, F, and K), and presence of differentiated cell types were confirmed by immunofluorescence microscopy and gene expression. Goblet, enteroendocrine, and Paneth cells were identified by staining for Muc2, Chromogranin A, and Lysozyme, respectively (Fig 3G-I). ZO-1 gene expression, indicating tight junction formation, was unchanged between spheroids and ODMs (Fig. 2B). Stem cell marker Lgr5 gene expression was significantly reduced in differentiated ODMs compared to spheroids. *Muc2* gene expression was significantly increased in ODMs compared to spheroid culture, and chromogranin A (*ChgA*) expression was elevated in ODMs, although not significantly (Fig. 2C-D). Altogether, these data confirmed differentiation of the ODMs after 2-3 days in DM. Turnover of the ODMs was also observed (Sup Fig. 1D). During media changes, dead cells were observed in spent media,

but the monolayers remained intact, indicating that dead cells that had sloughed off were likely replaced with new cells. The cell turnover rate appeared comparable to that of intestinal epithelium *in vivo* (2-3 days in mice and 3-5 days in humans) [19].

Differentiated monolayers infected with 10^6, 10^5, or 10^4 mNeonGreen expressing *C. parvum* oocysts were tracked over the course of 3 weeks with live widefield epifluorescence microscopy (representative images in Fig. 3L). The parasite vacuole load decreased slowly over the course of 3 weeks (Fig. 3M). By 21 dpi, PVs were still present, but they were no longer present in each field of view. Interestingly, the biggest drops in vacuole load were concurrent with supernatant collections (Fig. 3M). After an initial drop, the population often increased and leveled out until the next supernatant collection was performed. These trends occurred in multiple similar experiments (Sup Fig 1A-C). Over the course of the infection, an average of about 4.1 x10^5, 6.6 x10^4, and 2.3 x 10^4 PVs were estimated to have formed per monolayer based on calculating the area under the curve of PVs for the total infection course for 10^6, 10^5, or 10^4 infective doses, respectively, with the estimated total PVs for the 10^6 dose being significantly higher than the others (Fig. 3N). Oocysts collected from the supernatant of ODMs were quantified by flow cytometry (Fig. 3O). Even though the 10^6 infective dose resulted in a significantly higher number of estimated PVs (Fig 3M-N), this did not correlate with the number of oocysts produced (Fig 3O-P) compared to the smaller infective doses. In fact, oocyst output for each condition was comparable (Fig 3P). Oocyst counts did not directly increase with the drop in number of vacuoles observed after supernatant collection, likely because many of the host cells that sloughed off the monolayer were also infected (Sup Fig. 1D). Overall, organoid derived monolayers support robust infection with *C. parvum* and production of new oocysts.

Organoid derived monolayers support *C. parvum* mating. Organoid derived monolayers were coinfected with mNeonGreen (mNG) and tdTomato (tdT) reporter *C. parvum* strains and infections were observed and recorded with live imaging over the course of 3 weeks. Double positive vacuoles indicative of mating were present (Fig. 5A), but rare compared to single positive vacuoles (Fig. 4A-C). Oocyst output from ODMs can serve as a proxy for fertilization and total oocyst output from the 3 experiments was not statistically significantly different (Fig. 4G-H). New oocysts with single positive, double positive, and double negative phenotypes were also produced from these infections (Fig. 4D-F). Double positive oocysts were again rare events and were not observed in all supernatant collections (Fig. 4D-F, Fig 5B). While most of the oocyst population collected in supernatant from the ODMs was composed of double negative oocysts, we cannot confirm that they resulted from outcrossing because a high proportion of double negative oocysts were detected in the washes performed immediately after infection (Sup Fig. 3B). This suggested that they were present in the input. Upon retrospective examination of the tdT and mNG stocks used for these experiments, the mNG stock was confirmed to be a mixed population of mNG and

non-fluorescent oocysts. This means that in truth the results reflect the mixing of 3 phenotypes rather than 2 and that vacuole counts from epifluorescence microscopy lacked data for the double negative population and underrepresented the total parasite load. Regardless of the limitations, the presence of double positive vacuoles within the ODM and double positive oocysts in the supernatant combined with the total oocyst output confirm that fertilization and oocyst production is supported in organoid derived monolayers.

Discussion

These studies show that 2D and 3D organoid-based cultures generated using defined culture media contain differentiated cell types representative of intestinal epithelial tissue and support *Cryptosporidium* infection and sexual reproduction. Inverted enteroids support infection and subculture of *C. parvum* and organoid derived monolayers (ODMs) support *C. parvum* infection and new oocyst production for at least 21 days and enable studies of fertilization.

These organoid-based models represent the major cell types found in the small intestine and provide an environment that better mimics the *in vivo* environment. We confirmed the presence of enteroendocrine cells, goblet cells, Paneth cells, enterocytes, and stem cells by gene and protein expression, which aligns with reported data [12,18,20–22]. The presence of tuft cells and M cells was not confirmed here, but other groups have demonstrated them after adding media supplements to promote their differentiation [23,24]. We have observed cell turnover in both formats resembling cell turnover found in the gut *in vivo*, which occurs about every 3 days in the mouse intestine (3-5 in human intestine) [4,19,25–27]. In both formats, host cells sloughed off the monolayer and were replaced by new cells in both uninfected and infected conditions. We have not investigated whether turnover rate is affected by infection. Many cells that sloughed off ODMs or enteroids were infected by various stages of *C. parvum* (Sup Fig. 1Cf). Like many other protozoans, *Cryptosporidium* has been shown to inhibit host cell apoptosis through NFκB [28–33]. Based on previous studies in biliary epithelium, it may be that uninfected cells in proximity to infected cells are undergoing apoptosis despite prolonged survival of infected cells [34]. The use of permeable supports in the ODMs allows for the possibility of measuring signals, such as alarmins, PAMPs, DAMPs, etc., released by host cells. Investigations exploring detection and communication of infection by uninfected cells and other mechanisms of innate infection control could be performed using these systems. It would be interesting to determine if increased cell turnover in the epithelium may be an innate mechanism to expel *Cryptosporidium*, as is the case in some helminth infections [35].

Inverted enteroids supported infection and subculture of *C. parvum* and circumvented the need for microinjection required by previous 3D organoid models of *Cryptosporidium* infection [12,21]. Using

inverted enteroids rather than microinjection makes infecting numerous enteroids easier and increases throughput. Other 3D environments require specialized equipment such as hollow nanofibers or silk scaffolds [10,11,36,37]. We have shown that subculture of the parasite in 3D enteroids is possible, although with diminishing returns, likely due to low reinfection rates as indicated by a decrease in infection load over time. Merozoites may have trouble finding and migrating to a new host cell after egress in the 3D environment of inverted enteroids. In the gut lumen or apical-in enteroids, merozoites could fall in any direction and land on a new host cell without relying on motility mechanisms, while merozoites may fall to the bottom of the dish in the case of inverted enteroids. To increase oocyst output using this method, initial infection, reinfection by merozoite stages, and microgamete fusion with macrogamonts needs to be enhanced. Introducing intermittent agitation, media circulation, rocking, or simulated microgravity (rotary cell culture system) during culture may improve reinfection rates and facilitate higher parasite loads and oocyst output using this system [38,39]. If improved, this method could be used to "farm" *Cryptosporidium* strains, improve ability to subculture *C. parvum*, and reduce mouse usage to maintain *C. parvum* strains. The scalability and the ability to subculture *C. parvum* with these methods could open many doors such as evolutionary studies of drug resistance, or be applied to other infectious organisms such as *Toxoplasma* or *Giardia* (which have been shown to establish productive ODM infections), as has been done for *Eimeria* and *Shigella* [15,16,18]. One disadvantage of inverted enteroids is the inability to observe swelling due to increased fluid secretion into the lumen, which is possible with apical-in enteroids [40], but it is still possible to assess barrier integrity [15]. Inverting enteroid polarity causes less damage to the enteroid structure than infection methods involving mechanical disruption of apical-in enteroids that have been used to make the apical surface accessible to infective agents [41].

The ODM system provides another way to study *C. parvum* cell biology at the apical surface. The relative ease of using commercial permeable supports has been established for human, mouse, pig, and chicken ODMs [14,18,24,36]. Other methods use various tools to make scaffolding out of silk or laser ablated channels in basement membrane gel to support human intestinal epithelial culture, but they require significantly more effort and specialized equipment [19,26,27]. ODMs are ready for infection within 5 days, which more closely resembles the maturation, differentiation, and turnover in the intestine. This is 5-6 days faster than monolayers using the stem cell derived air-liquid interface (ALI) system used in a previously reported *Cryptosporidium* infection model [14]. Dispensing with irradiated feeder cells (3T3s) and an ALI simplifies the initiation and differentiation of the cultures and infection procedures. Instead, the stem cell niche is presumably maintained by signals provided by Paneth cells [42,43]. The defined media used here should not be subject to the same lot-to-lot variation inherent in fetal bovine serum-based media used for the ALI method, and thus be more reproducible. The ODM format also allows real-time observation of the infection as we have demonstrated in this study. Currently, the resolution is limited by

the working distance of the microscope objective, but we have measured relative size differences of parasitic vacuoles and observe expansion of the infection over time. Based on previously described methods, it could be possible to modify this for other formats to improve microscopy capabilities [20,22].

Our mating assay confirmed that ODMs support *C. parvum* fertilization *in vitro*. Double positive vacuoles indicated fusion of macrogamonts and microgametes. Double positive vacuoles were likely zygotes rather than the result of recombination offspring because both mNG and tdT genes were inserted on chromosome 5. The probability of successful recombination resulting in double positive parasites is low, but not impossible. The double positive vacuoles confirm that fertilization does indeed occur in ODMs. However, this mating assay method greatly underestimates the number of fertilization events because it fails to reflect the intrastrain fertilization events that would show single positive. Oocyst production as measured by flow cytometry is a proxy for intrastrain fertilization measurement. A previous study crossed a *C. parvum* strain constitutively expressing Cre recombinase with a strain with a floxed stop sequence preceding a tdNeon sequence to show that mating only occurred in the mouse intestine but not in HCT8s *in vitro*. However, their assay was also subject to the same underrepresentation of fertilization events in the mouse as our mating assay in the ODMs in this study [6]. Future studies devised to capture all fertilization events could help refine our understanding of the timing of fertilization, sporulation, and release of new oocysts which could yield new insight into aspects of the *Cryptosporidium* life cycle that could not easily be studied *in vitro*.

Two- and three- dimensional organoid-based methods supporting the complete lifecycle of *Cryptosporidium* have the potential to aid in making big strides toward understanding *Cryptosporidium*'s biology. This system can capitalize on the vast library of transgenic mice to generate organoids with the desired genotype and be used in tandem with genetic manipulation of *C. parvum* to interrogate both sides of the host-parasite interactions [44]. Transfection of the organoids has also been demonstrated by others if the desired host genotype does not exist [45]. Additionally, both formats could be used for co-culture with various immune cell types to facilitate *in vitro* studies of immune cell responses to infection [46,47]. Other studies have co-cultured various organoids or ODMs with T cells, intraepithelial lymphocytes, or macrophages [48–52]. Because this method is based on a protocol that makes shifting between host species simple with minor adjustments, it could facilitate the study of the basis of host-parasite specificity [18]. We are choosing to focus our future studies on understanding the differences between ODM- and cancer cell-based culture that enable *Cryptosporidium* fertilization.

Materials and Methods

Media Preparations

L-WRN conditioned media was prepared according to methods previously described [45]. Advanced DMEM/F12 supplemented with 20% FBS (vol/vol) was conditioned with stem cell maintenance ligands by culturing L-WRN cells for 12 days. L-WRN cells were engineered to overexpress Wnt3a, R-spondin, and noggin which help maintain and grow intestinal epithelial stem cells. Conditioned media was collected every 4 days and stored at -20°C.

Stem cell maintenance medium and differentiation medium (DM) were with supplemented with 10 mM nicotinamide, 1 mM N-acetylcysteine, 50 ng/mL mouse epidermal growth factor (R&D Systems 2028-EG), 1x Pen/strep, 2 mM GlutaMax, 1 mM HEPES, 1X N2 and 1X B27 supplements as described previously [18].

To prepare stem cell maintenance media (SCMM), L-WRN conditioned media was diluted to 50% in Advanced DMEM/F12 and the supplement cocktail described above was added. Differentiation media consisted of supplemented Advanced DMEM/F12 [18]. Five percent SCMM was prepared by diluting 50% SCMM with DM.

Intestinal Epithelial Stem Cell Isolation, Culture, and Maintenance: Stem cells were isolated for the small intestinal crypts of a C57Bl6/NJ mouse as described by Miyoshi et al [45]. Briefly, the mouse was euthanized and the small intestine was harvested, flushed with sterile PBS, opened lengthwise, scraped with a sterile glass slide to remove the villi, then minced and submerged in a collagenase solution (2 mg/mL collagenase type 1 and 50 ug/mL gentamicin in DMEM/F12). The tissue fragments were incubated at 37°C with vigorous pipette mixing every 10 minutes for 1 hour until the crypts had separated from larger tissue fragments. Isolated crypts were washed, resuspended in Matrigel™, and dropped on a cell culture plate to form domes. The plate was inverted during polymerization to prevent cell clusters from accumulating at the bottom of the Matrigel™ dom. Once polymerized, SCMM with 10 µM Y27632 inhibitor and 10 µM SB431542 was overlaid. SCMM with 500 nM A83-01 and 1 µM SB202190 added was changed every 2-3 days. For passage, spent media was aspirated, the Matrigel™ domes were washed with PBS, and then overlaid with Trypsin/EDTA and mechanically dissociated with a pipette. Spheroids were incubated with Trypsin/EDTA at 37°C for 2-5 minutes and then washed with washing medium (DMEM/F12, 10% FBS, 2 mM L-glutamine, 15 mM HEPES, and 1x pen/strep). Cells (usually a 1:5 passage) were centrifuged at 200 x g for 5 minutes. The supernatant was removed, and spheroids were resuspended in 2:1 Matrigel™ to SCMM and dotted onto plates to form domes, inverted, and incubated at 37°C until the Matrigel™ polymerized. SCMM was then overlaid on the Matrigel™ domes. Stem cell spheroids were passaged every 3-7 days depending on the size and density of the spheroids.

Organoid derived monolayer preparation: ODM preparation was done as described previously [18]**.** Spheroids were expanded appropriately to set up desired experiments. To prepare permeable supports, Matrigel™ diluted 1:10 in SCMM was added to desired wells and incubated overnight at 4°C. Prior to seeding diluted Matrigel™ suspension was removed from wells and wells were allowed to dry at 37°C for 10 minutes. To prepare mISCs for seeding spheroids were mechanically dissociated in Trypsin-EDTA with vigorous pipetting and incubated for 3-5 minutes at 37°C. Cells were then washed in washing medium and $3x10^5$ cells per permeable support were resuspended in 100 µL SCMM supplemented with 10 µM Y27632 inhibitor per well ($3x10^5$ cells/permeable support). After 24 hours, media was changed to 5% SCMM with 10 µM Y27632 inhibitor for 24 hours and then switched to differentiation medium without Y27632 inhibitor thereafter. After differentiating for 48 hours ODMs were ready for infection. ODMs were maintained with 5% CO_2 atmosphere at 37°C. Apical and basal media was changed every 2-3 days. Frequency of media change for apical chambers may have varied due to supernatant collections, and new media was added to apical chambers after supernatant collections.

Inverted enteroid preparation: Spheroids were maintained in stem cell maintenance media as described previously until spheroids reached 100-200 µm in diameter [17,18,45]. To invert the spheroids, media was replaced with ice cold 5 mM EDTA in PBS. The Matrigel™ dome was dislodged with a sterile plastic spatula to allow the dome to float in the buffer. Spheroids were incubated rocking at 4°C for 1 hour in 5 mM EDTA in PBS to depolymerize Matrigel™ and remove the basement membrane signals coming from the extracellular matrix. Meanwhile, wells set to receive the suspended spheroids were treated for anti-adhesion by coating with 4% BSA in PBS and incubating the plates at 37°C for at least 15 minutes. Pipette tips were precoated with 4% BSA in PBS before working with suspended enteroids to reduce adherence to the plastic. Spheroids were centrifuged at 200xg for 5 minutes, and gently washed and resuspended in DM to avoid shredding/sheering the spheroids. Resuspended spheroids were transferred to BSA treated wells and incubated for 2-3 days to allow cells to differentiate and reorient the apical surface to the outside. Twice daily, media and enteroids were gently resuspended to reduce adhesion the plate, discourage clumping of enteroids, and dislodge dead cells. Enteroids were maintained with a 5% CO_2 atmosphere at 37°C and were ready for use after 2-3 days. Media was changed every 2-3 days by centrifuging at 200xg for 5 minutes and resuspending in fresh DM.

Oocyst excystation procedure: Appropriate numbers of oocysts were disinfected with bleach (10%) for 10 minutes on ice. Oocysts were washed twice with PBS, incubated with 10 mM HCl at 37°C for 10 minutes, and centrifuged for 5 minutes at 14000xg and then resuspended in 2 mM sodium taurocholate and incubated at 37°C for 10 minutes before infection. Where specified, oocysts were allowed to excyst

for 1 hour in 2 mM sodium taurocholate at 37°C before being filtered through a 1 µm syringe filter to remove unexcysted oocysts and retain free sporozoites.

ODM *C. parvum* infection procedure: Stock oocysts were acquired from Bunchgrass Farms (*C. parvum* IOWA) or were expanded in mice with paromomycin selection prior to use (tdTomato and mNeonGreen oocysts, generous gifts from Boris Striepen's lab). Appropriate numbers of oocysts were excysted and incubated at 37°C for 10-30 minutes in sodium taurocholate and then added to warm media and dispensed into wells in 100 µL volumes. Sporozoites were allowed to infect for 2-3 hours in the incubator at 37°C before washing 3 times with PBS to remove unattached parasites.

***C. parvum* infection and subculture in inverted enteroids**: Differentiated enteroids to be infected were gathered and placed in anti-adhesion treated microcentrifuge tubes. Oocysts were excysted and sporozoites were added to media containing the enteroids. Enteroids were incubated with free sporozoites with intermittent agitation at 500-700 rpm for 1-2 hours at 37°C. Infected enteroids and media were then transferred to anti-adhesion treated wells. DNA, RNA, supernatant, and enteroid samples were collected at specified intervals. For enteroid subculture experiments, supernatants were collected from infected inverted enteroids 4 dpi by spinning down enteroids at 200xg for 5 minutes and collecting supernatants, which were subjected to the excystation procedure and used to infect fresh enteroids as above. This was repeated for 2 rounds, then enteroids were collected, fixed in 4% formaldehyde for 15-30 minutes, blocked in 4% bovine serum albumin and stained with FITC conjugated *Vicia Villosa* Lectin (1 µg/mL) for 1 hour at RT, and mounted whole on glass slides with Pro-Long Gold Antifade with DAPI.

ODM and Enteroid Immunofluorescence Assays and microscopy: Samples were fixed with 4% formaldehyde for 15 minutes at room temperature and then washed with PBS. Samples were permeabilized with 0.25% Triton X 100 in PBS for 10 minutes and then washed with PBS and blocked with 4% BSA in PBS overnight at 4°C. Samples were incubated with primary antibody at 5-10 ug/mL overnight at 4°C. Samples were washed with 4% BSA and secondary antibody was added at 2 ug/mL and incubated at room temperature for 1 hour washed and counterstained with 20 ug/mL Hoechst for 10 minutes. Enteroids were pelleted and resuspended in mounting medium and the suspension was mounted on glass slides. Stained ODMs were cut out of the supports with a razor blade and mounted on glass slides. Image acquisition was performed on a Nikon widefield epifluorescence microscope equipped with a 1.4-megapixel EXi blue CCD camera.

Supplemental Methods

Animal use: mNeonGreen and tdTomato *C. parvum* oocysts were maintained by infecting Nod/SCID/Gamma mice aged 3-6 weeks old with 10^5 mNeonGreen or tdTomato oocysts that were a kind

gift from the lab of Dr. Boris Striepen. Paromomycin was added to drinking water (16 mg/mL) and offered to mice ad libitum to select for mNeonGreen and tdTomato parasites. Fecal samples were collected for up to 3 months. Oocysts were isolated and purified from fecal samples using a sucrose floatation and cesium chloride gradient [52]. A C57Bl6/NJ mouse was euthanized and for mouse intestinal stem cells were isolated from the ileum. Animal experimentation and use was approved by the Institutional Animal Care and Use Committee of the University of Vermont (protocol X0-153).

RNA extraction and qRT-PCR: RNA extraction and purification from tissue culture was performed using RNeasy following manufacturer's instructions. RNA concentration was quantified, normalized, and then converted to cDNA using ThermoScientific High-Capacity cDNA kit. Expression of genes of interest (ChgA, Muc2, ZO-1) was assessed using SYBR Green PowerUp Mastermix and mRNA relative expression was normalized to GAPDH and calculated using the ΔΔCT method.

qPCR: DNA collection and purification from organoid derived monolayers (ODMs) and enteroids using the QIAmp DNA mini Kit. ODMs were scratched and mixed by pipetting in ATL Buffer and proteinase K for lysis and enteroids were collected by centrifugation and resuspended in ATL Buffer and proteinase K. Lysed samples were incubated at 56°C for 16-24 hours and then proceeded to column purification using manufacturer instructions. A standard curve was generated from a dilution series of purified *C. parvum* (Bunchgrass) DNA. Primer sequences for *C. parvum* 18S rRNA (forward: 5'-TAGAGATTGGAGGTTGTTCCT-3'; reverse: 5'-CTCCACCAACTAAGAACGGCC-3') were used for quantification. qPCR reactions were performed with *Power*SYBR Green, 2 uL of DNA template on a QuantStudio6 using these amplification conditions: 95°C 10 min, 40 cycles of 95°C 15 sec, 60°C 60 sec and a melt curve analysis. Genomic equivalents were determined by comparison to the standard curve.

Flow cytometry: Supernatants collected from ODMs were fixed in 4% formaldehyde for 15 minutes, permeabilized with Triton X 100 for 10 minutes, blocked with 4% BSA for 1 hour at RT, and stained with 5 µg/mL anti-COWP antibody overnight at 4°C. Samples were washed and stained with 2 µg/mL rabbit anti-mouse AF633 secondary antibody for 1 hour at RT. Samples were washed and resuspended in 1 mM EDTA in PBS and used for flow cytometry analysis on the MACSQuant VYB. Flow cytometric data analysis was done using FlowJo Software. Oocysts in supernatants were quantified using FSC/SSC gates to identify single cell populations of oocyst size by comparing to stock oocysts and identifying COWP+ cells. Subpopulations were determined based on mNeonGreen or tdTomato expression.

Live imaging/Microscopy: Infected cultures were removed from the incubator for periodic image collection at specified timepoints throughout the infection. A random sampling of tiled images (3x3-5x5) to cover approximately 10% of the permeable support's surface area were collected at 20x. Imaging was

performed on a Nikon widefield epifluorescence microscope equipped with a 1.4-megapixel EXi blue CCD camera. Images were analyzed to count parasitic vacuoles using a macro for Image J. Vacuoles counted for imaged area were then used to estimate the total number of vacuoles present on the total cell culture surface area.

Transmission Electron Microscopy: For preparation of ODMs, media from the apical and basal chambers was removed and replaced with Karnovsky's fixative (2.5% glutaraldehyde, 1% paraformaldehyde in 0.1M cacodylate buffer). Enteroids were pelleted by centrifugation at 200xg for 5 minutes and resuspended in Karnovsky's fixative. Samples were fixed for 2 hours or overnight at 4°C. ODMs and enteroids were washed with 0.1M cacodylate buffer. Samples were then post-fixed in 1% OsO_4 in 0.1M cacodylate buffer for 45 min at 4ºC, rinsed with cacodylate buffer, dehydrated in a graded ethanol series and embedded in Spurr's resin. Ultrathin sections were cut with a diamond knife, retrieved onto copper grids, and contrasted with uranyl acetate and lead citrate. Finally, the sections were imaged on a JEOL 1400 transmission electron microscope, and digital images acquired with an AMT XR611 high resolution 11-megapixel mid-mount CCD camera.

Statistical analysis: GraphPad Prism was used for all statistical analyses. Statistical significance was assessed with a two-tailed, unpaired t-test or One-Way ANOVA where p value ≤ 0.05 was considered significant. Error is shown as standard deviation and p-values are displayed on each graph. Statistical parameters are specified in figure legends.

Data Availability: Data are in the form of images and excel files with counts generated by macro analysis in Image J, qRT-PCR, or flow cytometry data. All data will be made available upon request via file transfer.

Acknowledgements

Funding for this study was provided by the Vermont Immunobiology and Infectious Disease Training Grant 2T32AI055402-16A1 and RO1AI143951.

We would like to thank the Harry Hood Bassett Flow Cytometry and Cell Sorting Facility (RRID:SCR_022147) at the University of Vermont Larner College of Medicine in the generation of our flow cytometry data.

Transmission electron microscopy sample preparation and imaging was performed at the Microscopy Imaging Center at the University of Vermont (RRID# SCR_018821).

The qPCR and qRT-PCR were performed using equipment in Vermont Integrative Genomics Resource DNA Facility and was supported by University of Vermont Cancer Center, Lake Champlain Cancer Research Organization, and the UVM Larner College of Medicine.

We would like to thank Dr. Christian Klotz for consultations while refining this protocol for *Cryptosporidium* infection, Dr. Boris Striepen for the generous gift of the tdTomato and mNeonGreen strains of *C. parvum*, and Camilla Strother and Ethan Mattice for their help during the initial stem cell isolations.

Figure 1A, 2A, and 3A were created with BioRender.com.

References

1. Dadonaite, B., Ritchie, H. & Roser, M. Diarrheal diseases. *Our World Data* (2018).
2. Kotloff, K. L. *et al.* Burden and aetiology of diarrhoeal disease in infants and young children in developing countries (the Global Enteric Multicenter Study, GEMS): a prospective, case-control study. *The Lancet* **382**, 209–222 (2013).
3. Troeger, C. *et al.* Estimates of global, regional, and national morbidity, mortality, and aetiologies of diarrhoeal diseases: a systematic analysis for the Global Burden of Disease Study 2015. *Lancet Infect. Dis.* **17**, 909–948 (2017).
4. Liu, J., Bolick, D. T., Kolling, G. L., Fu, Z. & Guerrant, R. L. Protein Malnutrition Impairs Intestinal Epithelial Cell Turnover, a Potential Mechanism of Increased Cryptosporidiosis in a Murine Model. *Infect. Immun.* **84**, 3542–3549 (2016).
5. English, E. D., Guérin, A., Tandel, J. & Striepen, B. Live imaging of the Cryptosporidium parvum life cycle reveals direct development of male and female gametes from type I meronts. *PLOS Biol.* **20**, e3001604 (2022).
6. Tandel, J. *et al.* Life cycle progression and sexual development of the apicomplexan parasite Cryptosporidium parvum. *Nat. Microbiol.* **4**, 2226–2236 (2019).
7. Upton, S. J., Tilley, M. & Brillhart, D. B. Comparative development of Cryptosporidium parvum (Apicomplexa) in 11 continuous host cell lines. *FEMS Microbiol. Lett.* **118**, 233–236 (1994).

8. Hijjawi, N. S., Meloni, B. P., Morgan, U. M. & Thompson, R. C. Complete development and long-term maintenance of Cryptosporidium parvum human and cattle genotypes in cell culture. *Int. J. Parasitol.* **31**, 1048–1055 (2001).
9. Miller, C. N. *et al.* A cell culture platform for Cryptosporidium that enables long-term cultivation and new tools for the systematic investigation of its biology. *Int. J. Parasitol.* **48**, 197–201 (2018).
10. Morada, M. *et al.* Continuous culture of Cryptosporidium parvum using hollow fiber technology. *Int. J. Parasitol.* **46**, 21–29 (2016).
11. Yarlett, N., Morada, M., Gobin, M., Van Voorhis, W. & Arnold, S. In Vitro Culture of Cryptosporidium parvum Using Hollow Fiber Bioreactor: Applications for Simultaneous Pharmacokinetic and Pharmacodynamic Evaluation of Test Compounds. *Methods Mol. Biol. Clifton NJ* **2052**, 335–350 (2020).
12. Heo, I. *et al.* Modeling Cryptosporidium infection in human small intestinal and lung organoids. *Nat. Microbiol.* **3**, 814–823 (2018).
13. Nikolaev, M. *et al.* Homeostatic mini-intestines through scaffold-guided organoid morphogenesis. *Nature* **585**, 574–578 (2020).
14. Wilke, G. *et al.* A Stem-Cell-Derived Platform Enables Complete Cryptosporidium Development In Vitro and Genetic Tractability. *Cell Host Microbe* **26**, 123-134.e8 (2019).
15. Co, J. Y., Margalef-Català, M., Monack, D. M. & Amieva, M. R. Controlling the polarity of human gastrointestinal organoids to investigate epithelial biology and infectious diseases. *Nat. Protoc.* **16**, 5171–5192 (2021).
16. Nash, T. J., Morris, K. M., Mabbott, N. A. & Vervelde, L. Inside-out chicken enteroids with leukocyte component as a model to study host–pathogen interactions. *Commun. Biol.* **4**, 1–15 (2021).
17. Stroulios, G. *et al.* Culture Methods to Study Apical-Specific Interactions using Intestinal Organoid Models. *J. Vis. Exp. JoVE* (2021) doi:10.3791/62330.

18. Holthaus, D., Delgado-Betancourt, E., Aebischer, T., Seeber, F. & Klotz, C. Harmonization of Protocols for Multi-Species Organoid Platforms to Study the Intestinal Biology of Toxoplasma gondii and Other Protozoan Infections. *Front. Cell. Infect. Microbiol.* **10**, (2021).
19. Barker, N. Adult intestinal stem cells: critical drivers of epithelial homeostasis and regeneration. *Nat. Rev. Mol. Cell Biol.* **15**, 19–33 (2014).
20. Luu, L. *et al.* An Open-Format Enteroid Culture System for Interrogation of Interactions Between Toxoplasma gondii and the Intestinal Epithelium. *Front. Cell. Infect. Microbiol.* **9**, (2019).
21. Dutta, D., Heo, I. & O'Connor, R. Studying Cryptosporidium Infection in 3D Tissue-derived Human Organoid Culture Systems by Microinjection. *J. Vis. Exp. JoVE* (2019) doi:10.3791/59610.
22. Hares, M. F. *et al.* Stem cell-derived enteroid cultures as a tool for dissecting host-parasite interactions in the small intestinal epithelium. *Parasite Immunol.* **43**, e12765 (2021).
23. Fasciano, A. C., Blutt, S. E., Estes, M. K. & Mecsas, J. Induced Differentiation of M Cell-like Cells in Human Stem Cell-derived Ileal Enteroid Monolayers. *JoVE J. Vis. Exp.* e59894 (2019) doi:10.3791/59894.
24. Jelinsky, S. A. *et al.* Molecular and Functional Characterization of Human Intestinal Organoids and Monolayers for Modeling Epithelial Barrier. *Inflamm. Bowel Dis.* **29**, 195–206 (2023).
25. Krndija, D. *et al.* Active cell migration is critical for steady-state epithelial turnover in the gut. *Science* **365**, 705–710 (2019).
26. Park, J. *et al.* Promotion of Intestinal Epithelial Cell Turnover by Commensal Bacteria: Role of Short-Chain Fatty Acids. *PLOS ONE* **11**, e0156334 (2016).
27. Cheng, H. & Leblond, C. P. Origin, differentiation and renewal of the four main epithelial cell types in the mouse small intestine. V. Unitarian Theory of the origin of the four epithelial cell types. *Am. J. Anat.* **141**, 537–561 (1974).

28. Chen, X. *et al.* Cryptosporidium parvum activates nuclear factor κB in biliary epithelia preventing epithelial cell apoptosis. *Gastroenterology* **120**, 1774–1783 (2001).

29. Carmen, J. C. & Sinai, A. P. Suicide prevention: disruption of apoptotic pathways by protozoan parasites. *Mol. Microbiol.* **64**, 904–916 (2007).

30. McCole, D. F., Eckmann, L., Laurent, F. & Kagnoff, M. F. Intestinal Epithelial Cell Apoptosis following Cryptosporidium parvum Infection. *Infect. Immun.* **68**, 1710–1713 (2000).

31. Heussler, V. T., Küenzi, P. & Rottenberg, S. Inhibition of apoptosis by intracellular protozoan parasites. *Int. J. Parasitol.* **31**, 1166–1176 (2001).

32. Nishikawa, Y., Makala, L., Otsuka, H., Mikami, T. & Nagasawa, H. Mechanisms of apoptosis in murine fibroblasts by two intracellular protozoan parasites, Toxoplasma gondii and Neospora caninum. *Parasite Immunol.* **24**, 347–354 (2002).

33. Mele, R., Gomez Morales, M. A., Tosini, F. & Pozio, E. Cryptosporidium parvum at Different Developmental Stages Modulates Host Cell Apoptosis In Vitro. *Infect. Immun.* **72**, 6061–6067 (2004).

34. Chen, X.-M., Gores, G. J., Paya, C. V. & LaRusso, N. F. Cryptosporidium parvum induces apoptosis in biliary epithelia by a Fas/Fas ligand-dependent mechanism. *Am. J. Physiol.-Gastrointest. Liver Physiol.* **277**, G599–G608 (1999).

35. Cliffe, L. J. *et al.* Accelerated Intestinal Epithelial Cell Turnover: A New Mechanism of Parasite Expulsion. *Science* **308**, 1463–1465 (2005).

36. Cardenas, D. *et al.* Two- and Three-Dimensional Bioengineered Human Intestinal Tissue Models for Cryptosporidium. *Methods Mol. Biol. Clifton NJ* **2052**, 373–402 (2020).

37. Chen, Y., Zhou, W., Roh, T., Estes, M. K. & Kaplan, D. L. In vitro enteroid-derived three-dimensional tissue model of human small intestinal epithelium with innate immune responses. *PloS One* **12**, e0187880 (2017).

38. Carpenedo, R. L., Sargent, C. Y. & McDevitt, T. C. Rotary suspension culture enhances the efficiency, yield, and homogeneity of embryoid body differentiation. *Stem Cells Dayt. Ohio* **25**, 2224–2234 (2007).

39. Ryu, N.-E., Lee, S.-H. & Park, H. Spheroid Culture System Methods and Applications for Mesenchymal Stem Cells. *Cells* **8**, 1620 (2019).

40. Saxena, K. *et al.* Human Intestinal Enteroids: a New Model To Study Human Rotavirus Infection, Host Restriction, and Pathophysiology. *J. Virol.* **90**, 43–56 (2015).

41. Blutt, S. E. & Estes, M. K. Organoid Models for Infectious Disease. *Annu. Rev. Med.* **73**, 167–182 (2022).

42. Sato, T. *et al.* Paneth cells constitute the niche for Lgr5 stem cells in intestinal crypts. *Nature* **469**, 415–418 (2011).

43. Sato, T. *et al.* Single Lgr5 stem cells build crypt-villus structures in vitro without a mesenchymal niche. *Nature* **459**, 262–265 (2009).

44. Vinayak, S. Recent advances in genetic manipulation of Cryptosporidium. *Curr. Opin. Microbiol.* **58**, 146–152 (2020).

45. Miyoshi, H. & Stappenbeck, T. S. In vitro expansion and genetic modification of gastrointestinal stem cells in spheroid culture. *Nat. Protoc.* **8**, 2471–2482 (2013).

46. Schreurs, R. R. C. E., Baumdick, M. E., Drewniak, A. & Bunders, M. J. In vitro co-culture of human intestinal organoids and lamina propria-derived CD4+ T cells. *STAR Protoc.* **2**, 100519 (2021).

47. Read, E., Jowett, G. M., Coman, D. & Neves, J. F. Co-Culture of Murine Small Intestine Epithelial Organoids with Innate Lymphoid Cells. *J. Vis. Exp. JoVE* (2022) doi:10.3791/63554.

48. Wagar, L. E. *et al.* Modeling human adaptive immune responses with tonsil organoids. *Nat. Med.* **27**, 125–135 (2021).

49. Cook, L. *et al.* Suppressive and Gut-Reparative Functions of Human Type 1 T Regulatory Cells. *Gastroenterology* **157**, 1584–1598 (2019).

50. Rogoz, A., Reis, B. S., Karssemeijer, R. A. & Mucida, D. A 3-D enteroid-based model to study T-cell and epithelial cell interaction. *J. Immunol. Methods* **421**, 89–95 (2015).

51. Noel, G. *et al.* A primary human macrophage-enteroid co-culture model to investigate mucosal gut physiology and host-pathogen interactions. *Sci. Rep.* **7**, 45270 (2017).

52. Nozaki, K. *et al.* Co-culture with intestinal epithelial organoids allows efficient expansion and motility analysis of intraepithelial lymphocytes. *J. Gastroenterol.* **51**, 206–213 (2016).

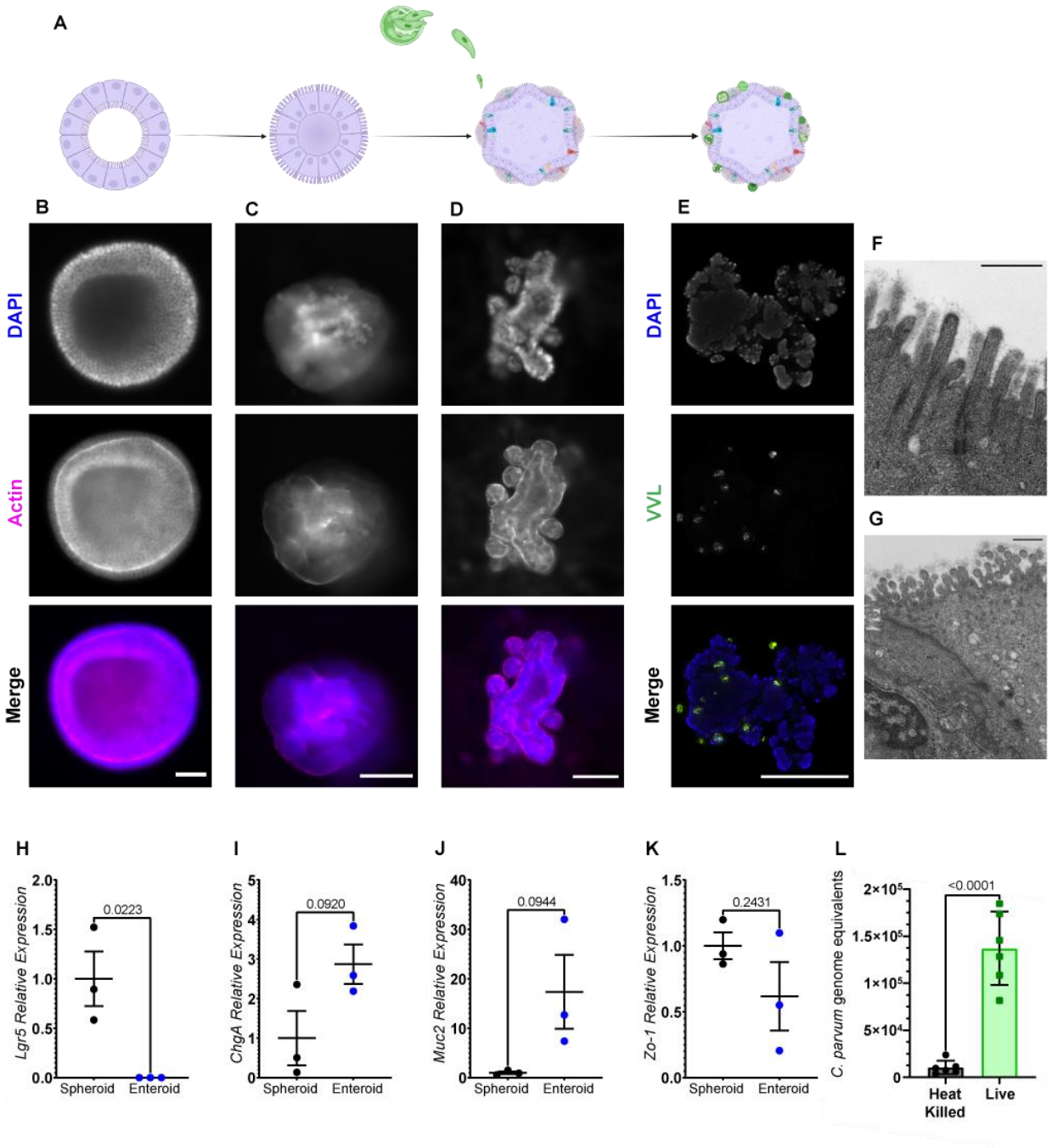

Fig. 1. Inverted, differentiated enteroids exhibit characteristics of the intestinal epithelium and allow infection with *C. parvum* without the need for microinjection. (**A**) Schematic of enteroid inversion, differentiation, and infection. Spheroids were incubated with 5 mM EDTA in PBS on a rocking platform for 1 hour at 4° C then resuspended in differentiation medium. Enteroids were differentiated for 2-3 days and then infected by adding free sporozoites to the media incubating with intermittent agitation for 1-2 hours. Infected enteroids were harvested at the desired timepoints for various analyses. (**B-D**) Immunofluorescent staining for actin with Phalloidin-Alexa Flour 647 (magenta) to mark the brush border and DAPI (blue) for host cell nuclei of an uninverted, undifferentiated enteroid (**B**), an inverted,

undifferentiated enteroid 1 day post inversion (**C**), and an inverted, differentiated enteroid 5 dpd (days post differentiation) (**D**). Scale bars are 50 µm. (**E**) Maximum intensity projection of infected inverted, differentiated enteroid 7 dpi stained with FITC conjugated *Vicia Villosa* Lectin (VVL; green) and DAPI (blue). Scale bar is 50 µm. (**F-G**) TEM micrograph of microvilli on surface (**F**) and tight junction (**G**) of an inverted enteroid 7 dpd. Scale bar is 500 nm. (**H-K**) qRT-PCR comparing mRNA expression of stem cell marker Lgr5 (**H**), enteroendocrine marker Chromogranin A (ChgA) (**I**), goblet cell marker Muc2 (**J**), and tight junction marker ZO-1 (**K**) in spheroids and inverted, differentiated enteroids 3 dpd. Results are averages of 2 technical replicates from 3 experiments. (**L**) qPCR measuring genomic equivalents of heat killed or live *C. parvum* enteroid infections 7 dpi. Representative results from 1 experiment with 6 technical replicates are shown. Statistical significance was assessed with a two-tailed, unpaired t-test where p value ≤ 0.05 was considered significant. Error shown as standard deviation and p-value is displayed on graph.

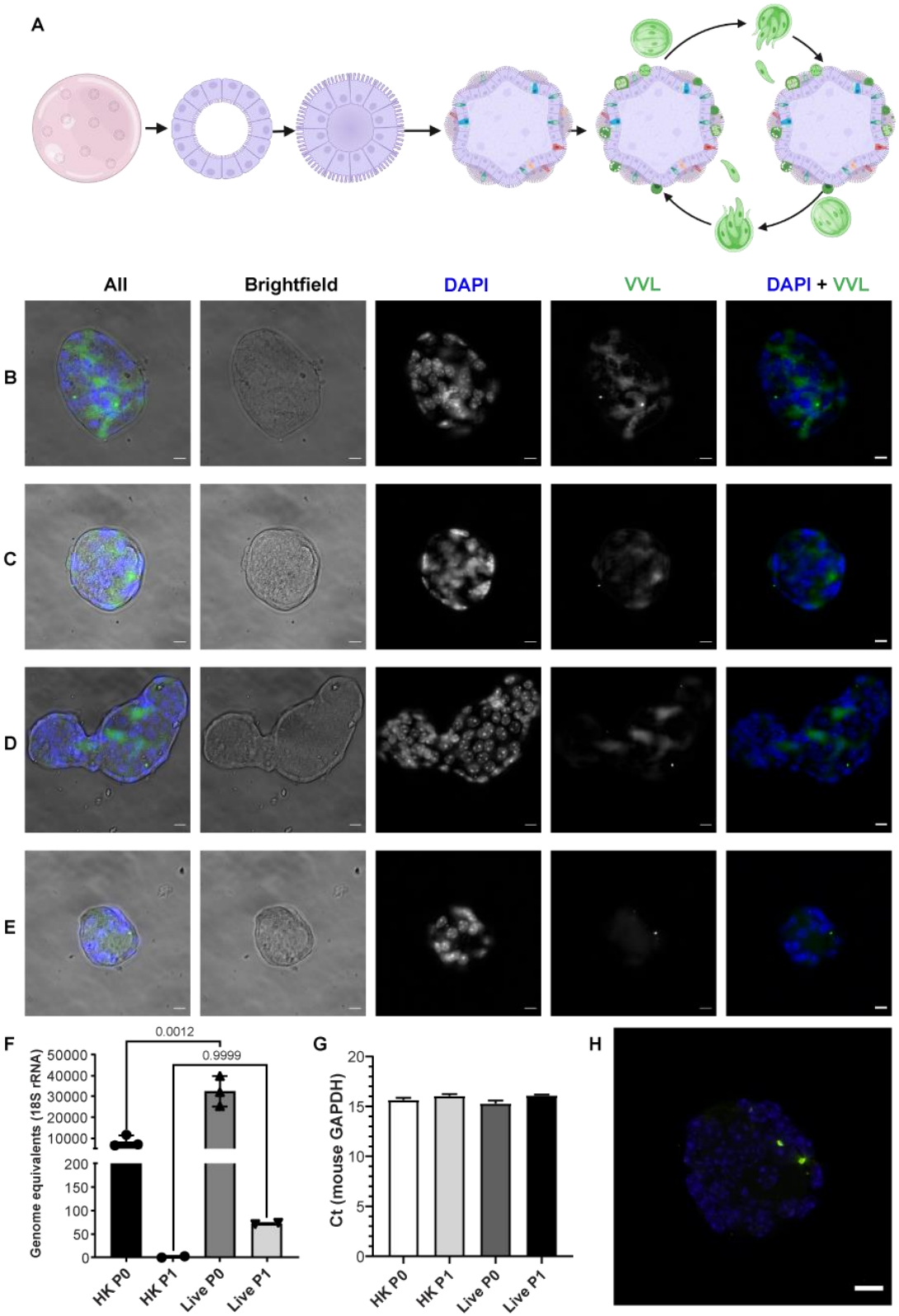
A
All
Brightfield
DAPI
VVL
DAPI + VVL
B
C
D
E
F
0.0012
0.9999
Genome equivalents (18S rRNA)
50000
40000
30000
20000
10000
200
150
100
50
0
HK P0
HK P1
Live P0
Live P1
G
Ct (mouse GAPDH)
20
15
10
5
0
HK P0
HK P1
Live P0
Live P1
H

Fig. 2. Successful subculture of *C. parvum* in inverted enteroids. (**A**) Schematic of subculture process in inverted enteroids. Spheroids were inverted and resuspended in differentiation medium and allowed to differentiate for 2 days. Inverted, differentiated enteroids (~50/well) were infected with 5 x 10^4 *C. parvum* oocysts/well. Oocysts were excysted, filtered through a 2 µm syringe filter to remove unexcysted oocysts, and free sporozoites were added to the medium. Sporozoites and enteroids were incubated at 37°C for 1-2 hours with intermittent agitation. New oocysts were collected from P0 supernatant 4 dpi and excysted to infect fresh enteroids (P1). Three dpi in the first passage supernatant was collected and used to infect P2. (**B-E**) Infected enteroids after 2 rounds of subculture in enteroids. After 2 rounds of subculture, enteroids were fixed 4dpi and parasite vacuoles were stained with FITC-VVL (green), and host nuclei are stained with DAPI (blue). (**F**) PCR quantification of parasite 18s rRNA gene in initial infection and first passage. (**G**) Ct values of mouse GAPDH to show relative host cell numbers remained consistent from one passage to another. (**H**) Maximum intensity projection of deconvolved z-stack on infected enteroid stained with FITC-VVL (green) and DAPI (blue). Scale bars are 10 µm.

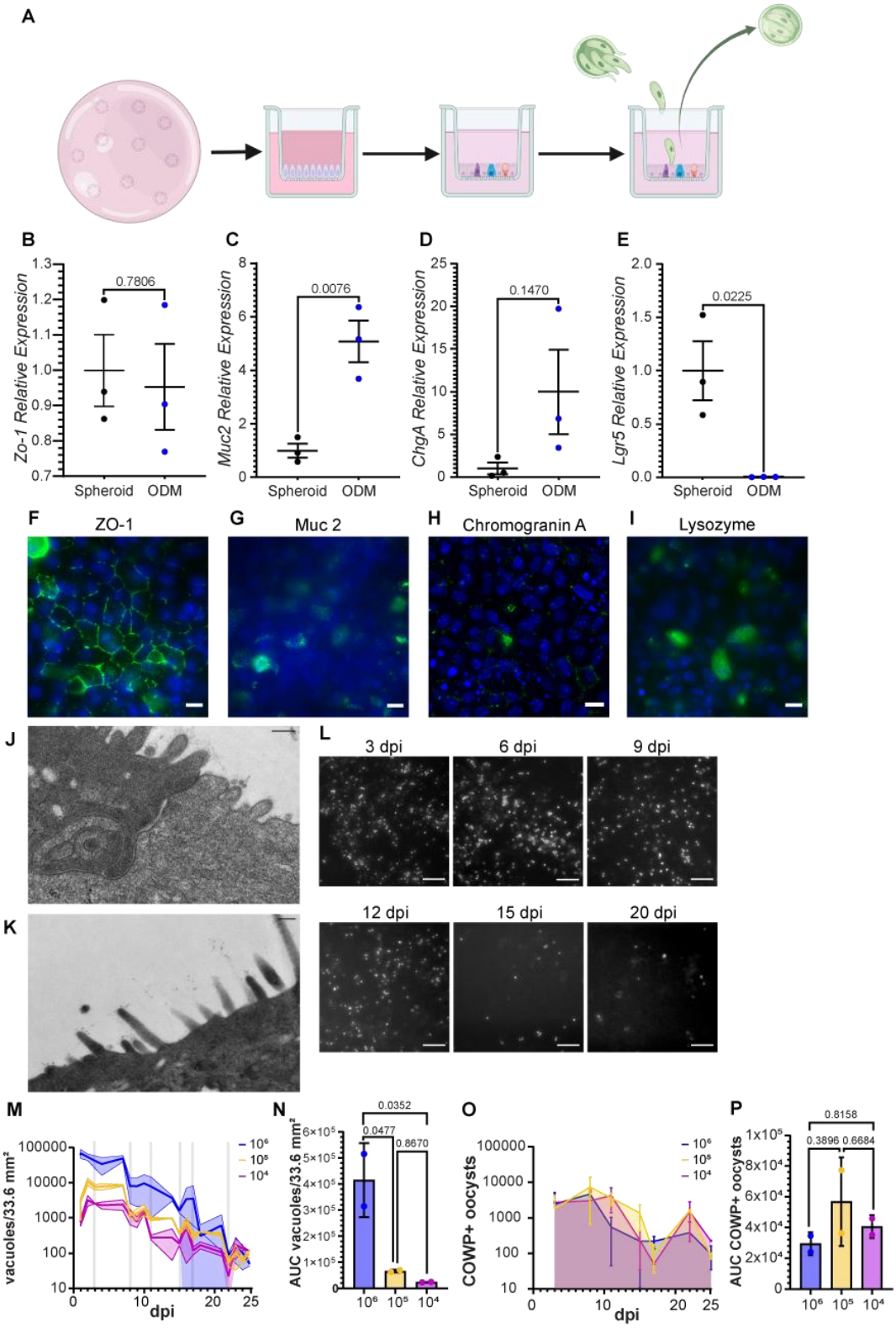

Fig. 3. Organoid derived monolayers exhibit intestinal epithelium characteristics and support *C. parvum* infection. (**A**) Schematic for organoid derived monolayer (ODM) differentiation and infection.

Mouse intestinal stem cells (mISC) were embedded and grown in Matrigel domes and maintained as spheroids in stem cell maintenance media (SCMM) until expanded enough to seed permeable supports. Prior to seeding, permeable supports were coated with a 1:10 Matrigel in SCMM and incubated overnight at 4°C. Matrigel dilution was removed and permeable supports were incubated at 37°C for at least 15 minutes prior to seeding with mISC. Permeable supports were seeded with $3x10^5$ cells/well in order to reach confluency within 24 hours. If there were not enough mISCs available to put excess cells into each well the mISC monolayer was maintained in SCMM until confluency was reached. Once confluent, the SCMM concentration was reduced to 5% for 24 hours, then monolayers were switched to differentiation media (DM) which lacked L-WRN conditioned media entirely. Organoid derived monolayers (ODM) were maintained in DM for 2-3 days and then infected with *C. parvum*. (**B-E**) qRT-PCR of mRNA expression of ZO-1 for tight junctions (**B**), Muc 2 for goblet cells (**C**), ChgA for enteroendocrine cells (**D**), and lgr5 for stem cells (**E**). A Student's t-test was used to assess statistical significance with a cut-off of 0.05. P-values are displayed on each graph. (**F-I**) Immunofluorescent staining of ZO-1 (**F**), Muc 2 (**G**), Chromogranin A (**H**), and Lysozyme (**I**) in green and nuclei in blue confirming the presence of tight junctions, goblet cells, enteroendocrine cells, and Paneth cells respectively in differentiated ODMs. (**J-K**) TEM confirmation of tight junction (**J**) and microvilli (**K**) on ODMs. Scale bars are 200 nm. (**L**) Representative live epifluorescence images of ODM infection with mNeonGreen parasites 3, 6, 9, 12, 15, and 20 dpi. Scale bar is 50 µm. (**M**) Vacuole counts from image J macro analysis of fluorescent parasite vacuoles adjusted for total cell culture area. Lines represent infection with different infectious doses (10^6 oocysts (blue), 10^5 oocysts (yellow) and 10^4 oocysts (magenta). Vertical grey lines show days with supernatant collection (3, 8, 11, 15, 17, 22, and 25 dpi); images were collected after supernatants were collected. Standard deviation is shown as shaded area surrounding each line. (**N**) Area under the curve (AUC) of experiment in M. (**O**) Flow cytometry quantification of COWP1 + oocysts collected from ODM supernatant. (**P**) AUC of oocyst counts in O. One-way ANOVA (Tukey post-hoc multiple comparisons) was used to assess statistical significance of AUC in N and P with a p-value cut-off of 0.05. P-values are displayed on graphs. Error bars show standard deviation. n=2 for each condition.

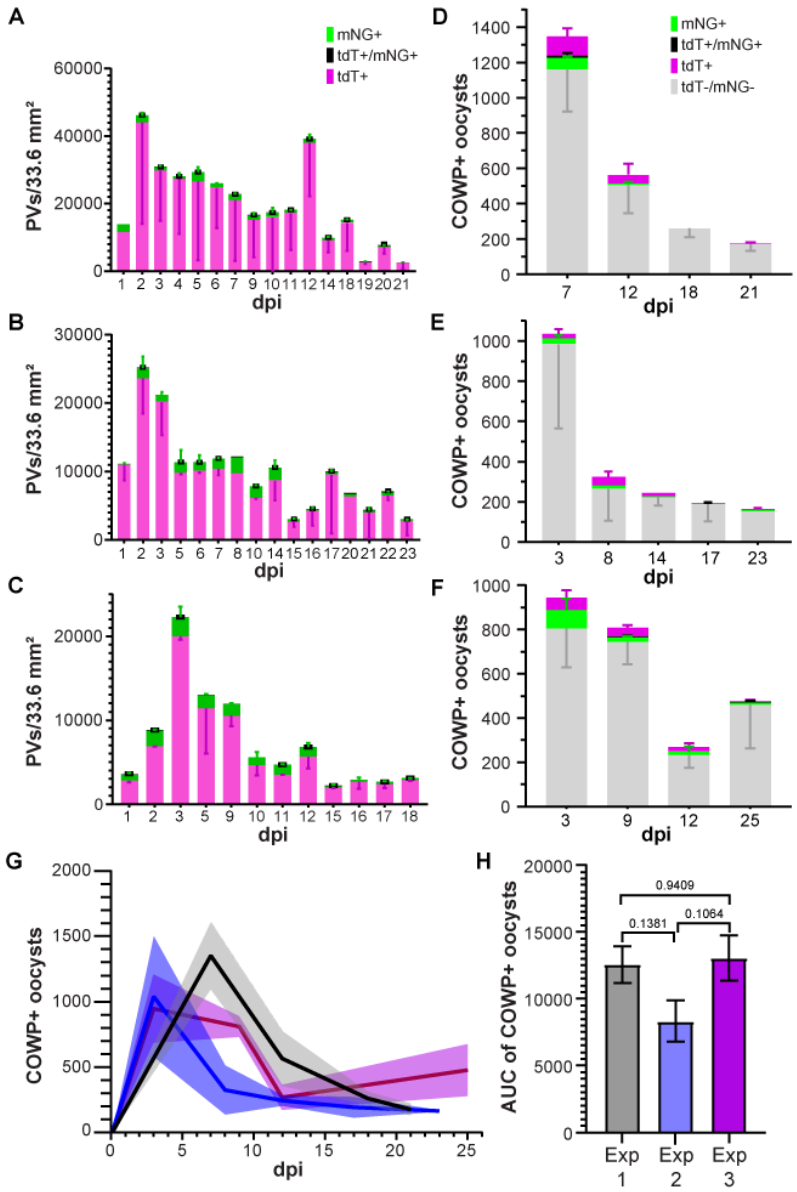

Fig. 4. Successful mating of two transgenic *C. parvum* strains in organoid derived monolayers. (**A-C**) Quantification of parasitophorous vacuoles (PVs) from Image J macro adjusted for total cell culture area. Each graph shows results from a different experiment. (**D-F**) Flow cytometry quantification of total oocysts collected from supernatant. Each graph shows oocyst results from individual experiments in A-C respectively. Error bars show standard deviation. (**G**) Total COWP1+ oocysts from supernatant over the course of the experiment. Each line represents a different experiment. Standard deviation is shown as shaded area surrounding each line. (**H**) AUC of COWP1+ oocysts for each experiment shown. One-way ANOVA (Tukey post-hoc multiple comparisons) used to assess statistical significance. P-values are displayed on graph. P-values ≤ 0.05 were considered significant. Error bars show standard deviation. n=2 for each experiment. Data is representative of 2 experiments.

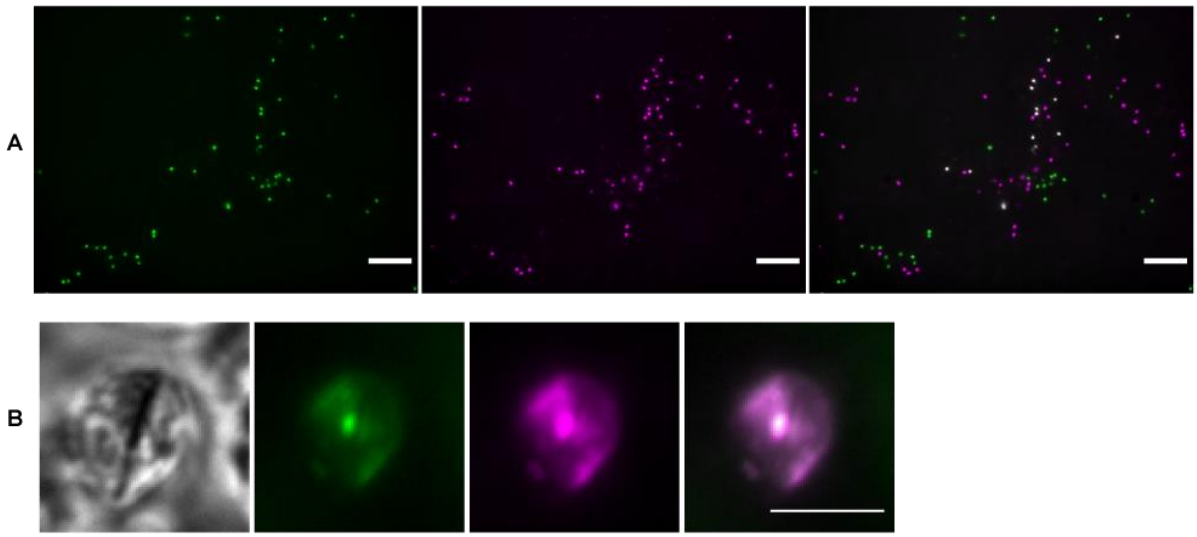

Figure 5. Inter-strain mating confirmed by double positive zygote and oocyst observation. (**A**) Live image of ODM infected with mNeonGreen (mNG) (left) and tdTomato (tdT) (middle) expressing *C. parvum* strains 8 dpi. Merge on the right shows double positive vacuoles in white. Scale bar is 50 µm. Image was processed for 2D deconvolution using AutoQuant X. (**B**) Oocyst collected from supernatant expressing both mNG and tdT. Scale bar is 5 µm.

Supplemental Figures

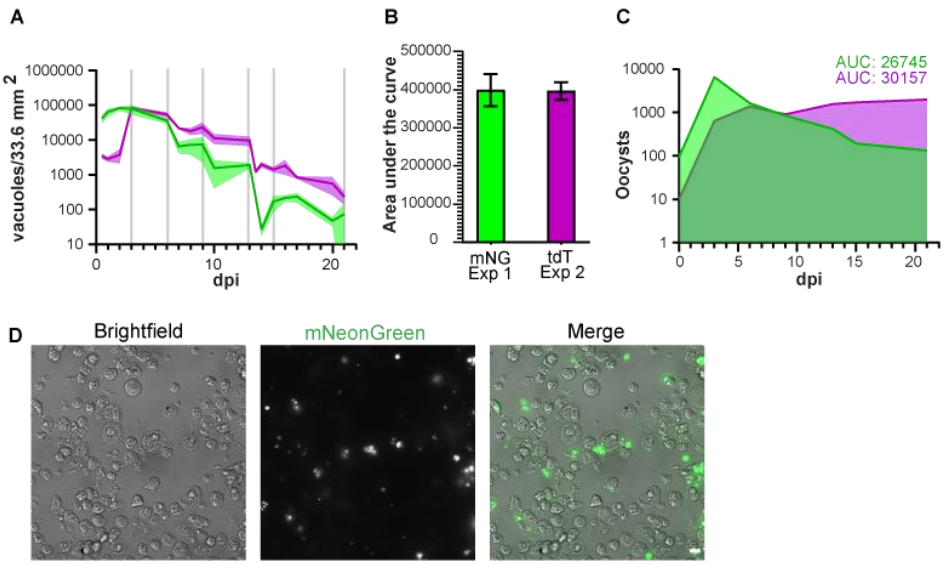

Supplemental Figure 1. (**A**) Vacuole counts from image J macro analysis of fluorescent parasite vacuoles adjusted for total cell culture area. Each colored line represents a different experiment. mNG infection (green) and tdT infection (magenta). Vertical grey lines show days with supernatant collection; images were collected before supernatants were collected. Standard deviation is shown as shaded area surrounding each line. (**B**) Area under the curve (AUC) of experiments in A. (**C**) Flow cytometry quantification of oocysts collected from ODM supernatant based on FSC and SSC of purified WT stock oocysts and expression of mNG or tdT. (**D**) Images of supernatant collected from ODMs infected with mNeonGreen expressing parasites 6 dpi. Dead host cells that have sloughed off the monolayer can be observed as well as various parasite stages (green). Parasites are observed to still be attached to host cells in many cases. Scale bar is 5 µm.

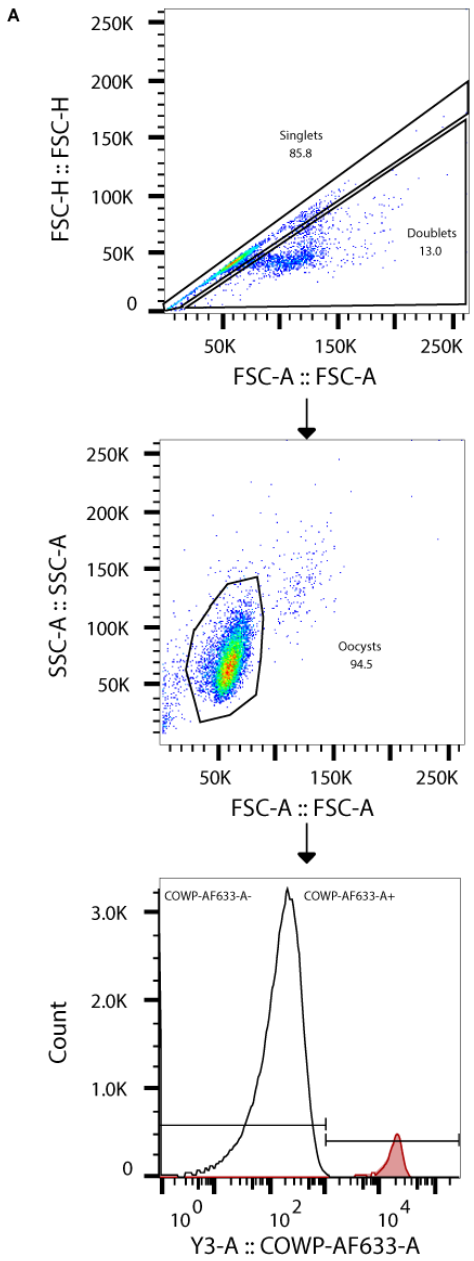

	Sample Name	Subset Name	Count
☐	BM2022-10-11_unstained oocysts.0001.fcs	Oocysts	150059
■	BM2022-10-11_stained oocysts.0001.fcs	Oocysts	8108

Supplemental Figure 2. Gating strategy for oocysts used for data in figure 3. Doublet discrimination was performed, then FSC and SSC were used to find oocyst size and granularity based on WT stock oocysts. Then COWP1 expression was used to confirm cells were oocysts. This figure was prepared with FlowJo and Adobe Illustrator.

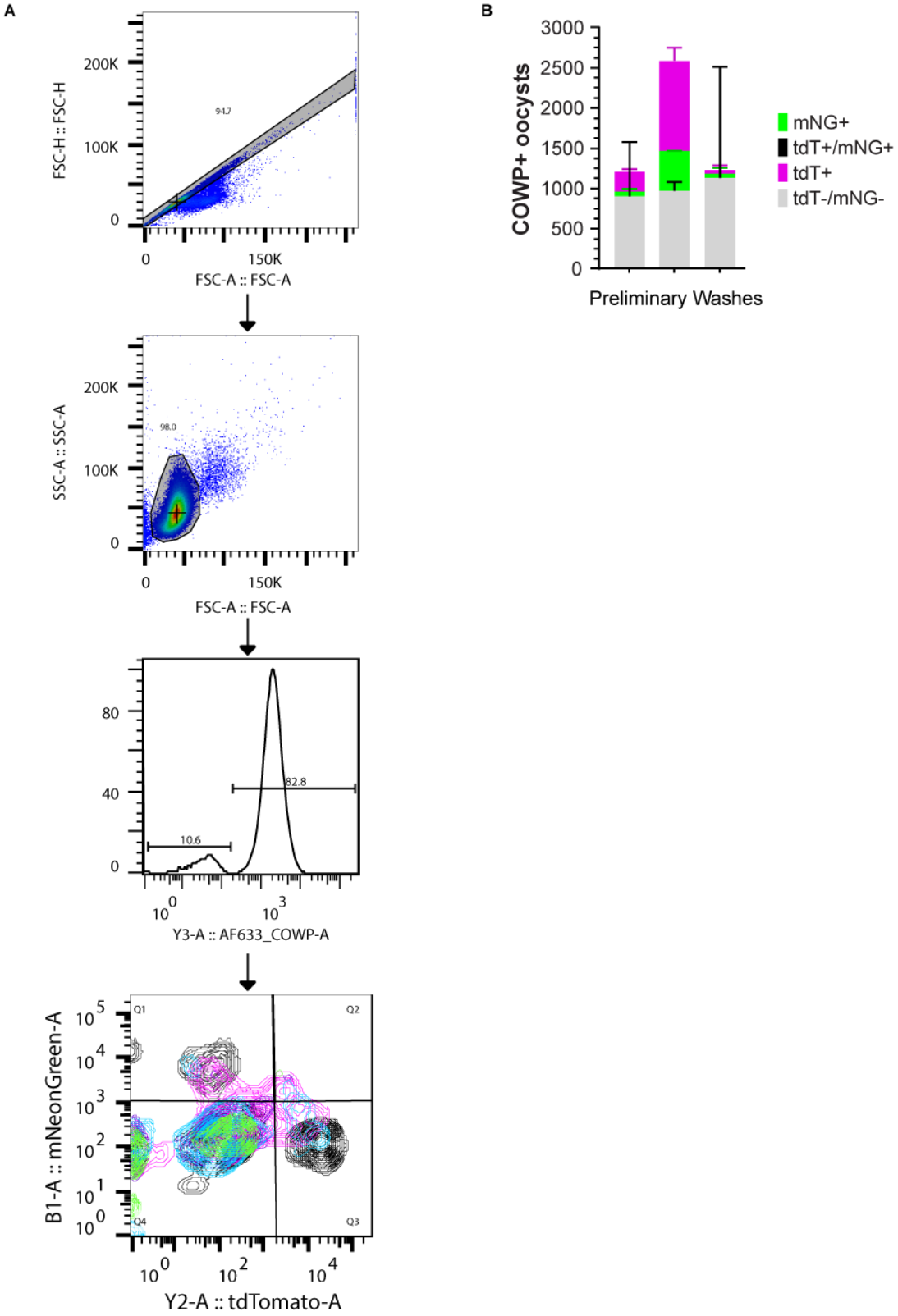
A
FSC-H :: FSC-H
200K
100K
0
94.7
0
150K
FSC-A :: FSC-A
SSC-A :: SSC-A
200K
100K
0
98.0
0
150K
FSC-A :: FSC-A
80
40
0
82.8
10.6
10^0
10^3
Y3-A :: AF633_COWP-A
B1-A :: mNeonGreen-A
10^5
10^4
10^3
10^2
10^1
10^0
Q1
Q2
Q4
Q3
10^0
10^2
10^4
Y2-A :: tdTomato-A
B
COWP+ oocysts
3000
2500
2000
1500
1000
500
0
Preliminary Washes
mNG+
tdT+/mNG+
tdT+
tdT-/mNG-

Supplemental Figure 3. (**A**) Gating strategy used to measure oocyst populations in figure 4. Doublet discrimination followed by gating on FSC and SSC based on purified stock WT oocysts, then COWP1 expression to identify oocysts. To assess the subpopulations of oocysts mNeonGreen and tdTomato expression was used to identify single positive, double positive, and double negative populations. Contour plots of samples with mixed populations are shown in different colors in the last panel. (**B**) Oocyst counts from the washes done 3 hpi to remove unexcysted oocysts and unattached parasites. Washes show that either the tdT or mNG oocyst stock was either contaminated with WT or reverted to WT at some point. The mixed population of non-fluorescent and mNG oocysts in the mNG oocyst stock was visually confirmed by looking at the stock microscopically. Visual inspection of the tdTomato stock showed a pure population. This explains why the majority of the PVs counted by ImageJ macro in figure 4 were tdT positive and that the macro counts significantly underestimate the PV count in the ODM. There was also likely crossing between WT and mNG or tdT that could not be distinguished from tdT x tdT or mNG x mNG crossing in this assay.

Supplemental Materials List

Material	Vendor	Product #
Advanced DMEM/F12	Gibco	12634028
Nicotinamide	Millipore	481907
N-acetylcysteine	Sigma	A9165
mouse epidermal growth factor	R&D Systems	2028-EG
Penicillin/streptomycin	Corning	30-002-Cl
GlutaMax	Gibco	35050061
HEPES	Gibco	15630-080
N2 supplement	Gibco	17502048
B27 supplement	Gibco	17504044
Matrigel™	Corning	CB40234
Y27632 inhibitor	R&D Systems	125450
SB 431542	R&D Systems	16141
A83-01	Sigma	SML0788
SB 202190	SYNthesis	SYN-1073
0.25% Trypsin/EDTA	Gibco	25200-056
High Capacity RNA-to-cDNA Kit	Applied Biosystems	4387406
RNeasy	QIAGEN	74104
PowerUp Mastermix	Applied Biosystems	4367659
QIAmp DNA mini Kit	Qiagen	51306
ThinCert Tissue Culture inserts	Greiner Bio-one	662 641
Fetal bovine serum, H.I.	Sigma	12306C, Lot 17H093
Fluorogel	Electron Microscopy Science	17985-10
Prolong Antifade Gold	Invitrogen	936941
EDTA (pH 8.0)	Promega	V4231
4% Paraformaldehyde	ThermoScientific	J19943-K2
DAPI	AppliChem	A4099, 0010
Hoescht	AnaSpec Inc.	AS-83219
Bovine Serum Albumin	Sigma	A7906
Triton-X-100	Promega	H5142
Tween 20	Fisher Bioreagents	BP337-500
MicroAmp Optical Reaction plates	Applied Biosystems	4309849
1 µm Syringe filter	Sartorius	

Cell lines		
L-WRN	ATCC (Miyoshi et. al 2013)	CRL-3276

C57Bl6/NJ intestinal stem cells	Isolated in Huston lab	NA

Equipment		
MACSQuant VYB	Miltenyi Biotec	Harry Hood Bassett Flow Cytometry and Cell Sorting Facility, UVM
QuantStudio6	Applied Biosystems	Vermont Integrative Genomics Resource DNA Facility, UVM
JEOL 1400 transmission electron microscope	JOEL	Microscopy Imaging Center, UVM

Parasites	
C. parvum	Bunchgrass Farms
tdTomato *C. parvum*	gift from Striepen Lab
mNeonGreen *C. parvum*	gift from Striepen Lab

Software	
ImageJ 1.53k	NIH
Adobe Illustrator	Adobe
FlowJo 10.8.0	BD
QuantStudio 1.3	Applied Biosystems
MS Excel 2010	Microsoft
GraphPad Prism 10	GraphPad

Antibodies/stains	Host	Source	Product #
Anti-ChgA	mouse	Proteintech	60135-1-Ig
Anti-Lysozyme	rabbit	Proteintech	15013-1-AP
Anti-Muc2	rabbit	Proteintech	27675-1-AP
Anti-ZO-1	mouse	Invitrogen	33-9100
Anti-COWP1	mouse	Invitrogen	MA183095
anti-Mouse, Alexa Fluor 488	Goat	LifeTechnologies	A11029
anti-Rabbit, Alexa Fluor 488	Donkey	LifeTechnologies	A21206
Alexa Fluor 633 phalloidin	NA	Invitrogen	A22284
FITC-VVL	NA	Vector Labs	FL-1231

	Target	Sequence 5'-3'	PrimerBank ID/Reference
housekeeping	mGapdh FWD	AGGTCGGTGTGAACGGATTTG	6679937a1
	mGapdh REV	TGTAGACCATGTAGTTGAGGTCA	
stem cell	mLgr5 FWD	CCTACTCGAAGACTTACCCAGT	6753842a1
	mLgr5 REV	GCATTGGGGTGAATGATAGCA	
enteroendocrine	mChgA FWD	ATCCTCTCTATCCTGCGACAC	6680932a1
	mChgA REV	GGGCTCTGGTTCTCAAACACT	
goblet cell	mMuc2 FWD	GCTGACGAGTGGTTGGTGAATG	Holthaus et al., 2021
	mMuc2 REV	GATGAGGTGGCAGACAGGAGAC	
tight junction	mZo1 FWD	GCCGCTAAGAGCACAGCAA	6678355a1
	mZo1 REV	TCCCCACTCTGAAAATGAGGA	
C. parvum	18S rRNA FWD	TAGAGATTGGAGGTTGTTCCT	NA
	18S rRNA REV	CTCCACCAACTAAGAACGGCC	